Theoretical transition probabilities for the OH Meinel system

Mark P. J. van der Loo and Gerrit C. Groenenboom[a)]
Theoretical Chemistry, Institute for Molecules and Materials, Radboud University Nijmegen, Toernooiveld 1, 6525ED Nijmegen, The Netherlands

(Received 12 December 2006; accepted 19 January 2007; published online 21 March 2007)

The authors present a new potential energy curve, electric dipole moment function, and spin-orbit coupling function for OH in the $X\,^2\Pi$ state, based on high-level *ab initio* calculations. These properties, combined with a spectroscopically parametrized lambda-type doubling Hamiltonian, are used to compute the Einstein A coefficients and photoabsorption cross sections for the OH Meinel transitions. The authors investigate the effect of spin-orbit coupling on the lifetimes of rovibrationally excited states. Comparing their results with earlier *ab initio* calculations, they conclude that their dipole moment and potential energy curve give the best agreement with experimental data to date. The results are made available via EPAPS Document No. E-JCPSAG-017709. © *2007 American Institute of Physics*. [DOI: 10.1063/1.2646859]

I. INTRODUCTION

The emission lines arising from rovibrationally excited hydroxyl radicals in the electronic ground state were first identified in the late 1940's by Meinel[1] in the airglow emission spectrum of the night sky. The Meinel emission lines have been used as a tool in studying many phenomena, including atmospheric temperature,[2] chemical lifetime of atmospheric OH,[3] atmospheric gravity waves,[4–6] extraterrestrial atmospheres,[7,8] and stellar oxygen abundance.[9]

Recently, we took part in a project[10,11] where the lifetime of vibrationally excited OH was for the first time measured directly by electrostatically decelerating and trapping OH radicals in the excited $X\,^2\Pi[v=1,J=3/2,f(+)]$ state and following the exponential decay in time. We computed the lifetime of excited OH based on a new *ab initio* dipole moment, took into account spin-orbit coupling and lambda-type doubling, and found good agreement with experiment. In the present work we extend our calculations to higher rovibrational levels and investigate the effect of including OH bond length dependent spin-orbit coupling. We compare our dipole moment function with several earlier ones and report a new set of Einstein A coefficients and photoabsorption cross sections for the OH Meinel system.

Experimentally, the emission rates are usually determined indirectly using nuclear wave functions computed from a parametrized potential and an electric dipole moment function which is fitted so that relative emission rates arising from different excited levels are reproduced. The electric dipole moment function is generally expanded in powers of the interatomic distance $(r-r_e)^n$, where r_e is the equilibrium distance and $n\geqslant 1$. Such a procedure was first followed by Shklovskii,[12] Chaimberlain and Smith,[13] and Kvifte.[14] They all took a linear dependence $(n=1)$ for the electric dipole moment functions. Heaps and Herzberg[15] and Wallace[16] used a quadratic function and Garvin *et al.*[17] a cubic function. In 1962, Ferguson and Parkingson[18] used a Morse potential, combined with experimental data from Krassovsky[19] to fit a fifth order polynomial for the electric dipole moment function. Murphy[20] improved on this model in 1971 using new experimental data. From 1982 onwards, the standard emission rates in spectroscopic databases[21] were those reported by Goldman and co-workers,[22–24] which were essentially based on a calculation by Mies.[25] In 1989, Turnbull and Lowe[26] reported emission rates based on a new empirical dipole moment function. However, it was recently noted by Cosby and Slanger[27] that the experimental data of Krassovsky *et al.*[28] underlying part of that fit is seriously flawed by modern standards. A new set of emission rates was published by Goldman *et al.*[29] in 1998, based on a Rydberg-Klein-Rees (RKR) potential of Nelson and Nesbitt.[30] The dipole moment function was obtained by combining an experimentally determined electric dipole moment function of Nelson *et al.*[31] with an *ab initio* dipole moment of Goldman *et al.*[29] An empirical spin-orbit coupling function by Coxon and Foster[32] was also included in that calculation. It was recently pointed out by Cosby *et al.*[33] and Colin *et al.*[34] that the spectroscopic constants used to generate the energy levels in the calculations of Goldman *et al.* are flawed at higher vibrational $(v>3)$ and rotational levels $(J>19/2)$, producing differences with experiment up to 0.14 cm^{-1}. Both authors performed an improved fit of existing spectroscopic data by Abrams *et al.*[35] The main disadvantage of experimentally determined electric dipole moment functions is that the regions outside the range of experimentally probed internuclear distances are badly described. Thus, extrapolation to higher rovibrational levels, which probe larger and smaller interatomic distances, is hardly possible.

The first extensive *ab initio* calculation of emission rates was done by Mies,[25] who used the electric dipole moment function of Stevens *et al.*[36] and an RKR potential of Albritton.[25] Extensive *ab initio* calculations of the electric dipole moment function of OH in the electronic ground state have been performed in the 1980's by Werner *et al.*[37] and Langhoff *et al.*[38,39] In 1986, Langhoff *et al.*,[40] reported the-

a)Author to whom correspondence should be addressed. Electronic mail: gerritg@theochem.ru.nl

TABLE I. Spectroscopic constants (Refs. 33 and 58) in cm^{-1} used in this work, see Eqs. (5)–(10).

v	A	$10^4 A_D$	$10^5 A_H$	B	q	$10^4 q_D$	$10^8 q_H$	p	$10^4 p_D$
0	−139.2729	−3.1626	−0.0285	18.550 404	−0.038 770	0.146 93	−0.243 06	0.235 608	−0.2483
1	−139.5410	−2.8334	−0.0275	17.838 640	−0.037 013	0.143 85	−0.227 56	0.225 097	−0.2548
2	−139.8057	−2.4002	−0.0285	17.136 383	−0.035 254	0.141 81	−0.225 78	0.214 261	−0.2555
3	−140.0608	−1.9303	−0.0248	16.440 990	−0.033 471	0.139 99	−0.222 73	0.203 253	−0.2604
4	−140.2964	−1.5181	−0.0255	15.749 203	−0.031 653	0.138 11	−0.194 75	0.191 693	−0.2684
5	−140.4982	−1.1026	−0.0247	15.056 955	−0.029 763	0.133 96	−0.100 96	0.179 474	−0.2806
6	−140.6433	−0.3809	−0.0238	14.359 026	−0.027 833	0.134 35	−0.078 81	0.166 648	−0.3187
7	−140.6984	0.4120	−0.0230	13.648 656	−0.025 786	0.133 08	0.000 00	0.152 240	−0.3574
8	−140.6137	2.4558	−0.0222	12.917 024	−0.023 621	0.136 83	0.000 00	0.136 138	−0.4360
9	−140.3060	5.8954	−0.0214	12.152 199	−0.021 267	0.141 47	0.000 00	0.117 007	−0.5361
10	−139.6458	11.7745	−0.0206	11.337 856	−0.018 522	0.127 78	0.000 00	0.093 326	−0.6915

oretical emission coefficients which were computed using a shifted version of the dipole moment function of Werner *et al.*[37] Nuclear wave functions were computed using an RKR potential, extended with *ab initio* calculations to describe the potential at large internuclear separations, and the Hill and van Vleck approximation was applied[41] to compute the transition probabilities. In all *ab initio* calculations and experimental fits mentioned here, the lambda-type doubling was neglected. Spin-orbit coupling effects were based on spectroscopic data and taken independent of the OH distance, except in the calculation by Goldman *et al.*[29]

II. THEORY

A. Hamiltonian and basis functions

The nuclear Hamiltonian for the OH molecule in the $X\,^2\Pi$ state can be written as

$$H = \frac{-\hbar^2}{2\mu r}\frac{\partial^2}{\partial r^2} r + T_{\mathrm{rot}} + V(r) + H_{\mathrm{so}}(r) + H_{\Lambda}, \tag{1}$$

where the first term is the radial part of the nuclear kinetic energy operator with r as the internuclear distance, μ is the reduced mass, and T_{rot} is the rotational Hamiltonian for OH in the $X\,^2\Pi$ state,

$$T_{\mathrm{rot}} = \frac{1}{2\mu r^2}[\mathbf{J}^2 + \mathbf{S}^2 + L_z(2S_z + L_z) - 2J_z(S_z + L_z) - (J_- S_+ + J_+ S_-)], \tag{2}$$

where $\mathbf{J}$ is the total angular momentum operator apart from nuclear spin, L_z is the body-fixed z component of the electronic orbital angular momentum operator $\mathbf{L}$, and $\mathbf{S}$ is the electronic spin operator. The full rotation Hamiltonian [given by $(\mathbf{J}-\mathbf{L}-\mathbf{S})^2$] also contains terms that couple the $X\,^2\Pi$ state with Δ and Σ states. These contributions are treated by the effective lambda-type doubling Hamiltonian H_{Λ}, in the unique perturber approximation.[42,43] The third term in Eq. (1) is the electronic potential energy surface in the clamped-nuclei approximation, and $H_{\mathrm{so}}(r)$ is the r-dependent spin-orbit coupling operator.

We represent the Hamiltonian in a Hund's case (a) basis with basis functions

$$|JM_J\,^2\Pi_{|\Omega|} p\rangle = (1/\sqrt{2})[|JM_J\,^2\Pi_{\Omega}\rangle + \eta(-1)^{J-S}|JM_J\,^2\Pi_{-\Omega}\rangle], \tag{3}$$

where

$$|JM_J\,^2\Pi_{\Omega}\rangle = \sqrt{\frac{2J+1}{4\pi}} D^{(J)*}_{M_J\Omega}(\alpha,\beta,0)|^2\Pi_{\Omega}\rangle. \tag{4}$$

Here, J is the total angular momentum quantum number, M_J is the projection of $\mathbf{J}$ on the laboratory-frame Z axis, $\Omega = \pm 1/2, \pm 3/2$ is the total electronic angular momentum projection on the molecular axis, and $\eta = \pm 1$ is the eigenvalue of the parity operator. We also introduce here the spectroscopic parity $p = \eta(-1)^{J-S}$, and we label wave functions with parity e or f for $p=1$ or $p=-1$, respectively. Furthermore, $\sqrt{(2J+1)/4\pi} D^{(J)*}_{M_J\Omega}(\alpha,\beta,0)$ is a two-angle normalized Wigner D function, and $|^2\Pi_{\Omega}\rangle$ denotes the electronic basis functions.

Spin-orbit coupling lifts the degeneracy of states with different $|\Omega|$. The transition probabilities depend on spin-orbit coupling because it affects the rovibronic energy level structure of the molecule and alters the shape of the nuclear vibrational wave functions. Spin-orbit coupling can be taken into account, either by computing the electronic expectation values of the r-dependent spin-orbit coupling operator $\hat{H}_{\mathrm{so}}(r)$ or by using a parametrized Hamiltonian matrix in the Hund's case (a) basis, of which the matrix elements $H^{\mathrm{so}}_{|\Omega|,|\Omega'|}$ are given by[42]

$$H^{\mathrm{so}}_{3/2,3/2} = \frac{A_v}{2} + \frac{A_{D_v}}{2}(z-1) + \frac{A_{H_v}}{4}[3(z-1)^2 + z], \tag{5}$$

$$H^{\mathrm{so}}_{1/2,3/2} = \frac{z^{1/2}}{2} A_{H_v}, \tag{6}$$

$$H^{\mathrm{so}}_{1/2,1/2} = -\frac{A_v}{2} - \frac{A_{D_v}}{2}(z+1) + \frac{A_{H_v}}{4}[3(z+1)^2 + z], \tag{7}$$

where $z = (J+1/2)^2 - 1$ and the A_n are spectroscopic constants, given in Table I. The spectroscopic spin-orbit Hamiltonian of Eqs. (5)–(7) reproduces the energy level structure, but does not affect the shape of nuclear wave functions, since terms dependent on r are averaged out. Thus, the Frank-

Condon overlap between different nuclear states is affected when Eqs. (5)–(7) are used instead of the r-dependent spin-orbit coupling. The calculation of the r-dependent spin-orbit coupling is described in Sec. II B.

The lambda-type doubling Hamiltonian lifts the degeneracy of states with different parities, and it is parametrized by spectroscopic constants. Its matrix elements $H^{\Lambda}_{|\Omega|,|\Omega'|}$ are given by[42]

$$H^{\Lambda}_{3/2,3/2} = \frac{z}{2}[q_v + x(q_{D_v} + xq_{H_v})], \tag{8}$$

$$H^{\Lambda}_{1/2,3/2} = z^{1/2}\left\{\frac{1 \mp (J+1/2)}{2}[q_v + x(q_{D_v} + xq_{H_v})] + \frac{1}{4}(p_v + xp_{D_v})\right\}, \tag{9}$$

$$H^{\Lambda}_{1/2,1/2} = \frac{z + 2 \mp 2(J+1/2)}{2}[q_v + x(q_{D_v} + xq_{H_v})] + \frac{1 \mp (J+1/2)}{2}(p_v + x) + \frac{A_v(p_v + xp_{D_v})}{8B_v}, \tag{10}$$

where p_v and q_v are lambda-type doubling constants, B_v rotational constants and $x=J(J+1)$. When two signs are given, the upper sign refers to e states and the lower sign to f states. We note that the last term in Eq. (10) is often labeled o_v.

B. Electronic structure and nuclear wave functions

The calculation of the electronic Born-Oppenheimer potential with the MOLPRO (Ref. 44) program package was described earlier by us.[45] Briefly, the electronic wave functions are obtained from an internally contracted multireference configuration interaction calculation with single and double excitations (MRSDCI).[46,47] The orbitals were obtained from a complete active space self-consistent field[48,49] (CASSCF) calculation with an extended active space consisting of five σ, two π_x, and two π_y orbitals, obtained from a large (aug-cc-pV6Z) one-electron basis set of Dunning.[50] Although our potential energy surface already gives accurate vibrational transition frequencies with deviations from experiment on the order of 0.1%, we decided to further increase the accuracy by replacing the potential with a scaled potential $V_{sc}(r)$ given by

$$V_{sc}(r) = c_3 V(c_0 + c_1 r + c_2 r^2). \tag{11}$$

Here, c_1, c_2, and c_3 are nonlinear scaling parameters, fitted to minimize the difference between the experimental and calculated vibrational levels G_v. Since the vibrational levels are not sensitive to the position of the minimum of the potential r_e, we introduce a shift c_0 so that r_e matches the experimentally determined value[51] of $1.8342a_0$. This method ensures that high quality nuclear wave functions are obtained for all rotational levels.

We compute the dipole moment as the expectation value of the electric dipole operator for the MRSDCI wave functions. The r-dependent spin-orbit coupling is obtained as the expectation value of the Breit-Pauli spin-orbit Hamiltonian, using wave functions obtained from MRSDCI calculations. The orbitals were obtained from a CASSCF calculation, using the aug-cc-pVQZ one-electron basis set and an active space formed by one π_x, one π_y, and six σ orbitals. The potential energy curve, spin-orbit coupling, and electric dipole moment function are computed at 30 points ranging from $1a_0$ to $16a_0$, and are made available via the EPAPS (Ref. 52) system.

The potential energy curve and electronic properties are interpolated using the reproducing kernel Hilbert space method[53] on an equidistant grid of 751 points between $1a_0$ and $16a_0$. The nuclear wave functions are obtained with the sinc-function discrete variable representation (sinc-DVR) method[54,55] employing this grid. The lambda-type doubling Hamiltonian is parametrized separately for every vibrational, rotational, and parity level, so we compute a new Hamiltonian matrix for every rovibrational and parity level. Furthermore, since the rotational and lambda-type doubling part of the Hamiltonian couple states of different Ω, the dimension of each Hamiltonian matrix doubles to 1502. After each diagonalization, 34 (17 for each Ω) or less bound state eigenfunctions are obtained. Only two of the eigenfunctions correspond to the rovibronic level for which the Hamiltonian was set up. These can be written as

$$|\psi^{JM_J}_{vF_np}\rangle = \sum_{|\Omega|} r^{-1} f^{J|\Omega|}_{vF_np}(r)|JM_J\ {}^2\Pi_{|\Omega|}p\rangle, \tag{12}$$

where the $r^{-1}f^{|\Omega|}_{vF_np}(r)$are the vibrational wave functions. The functions $|\psi^{JM_J}_{vF_np}\rangle$ are linear combinations of states with $|\Omega|=3/2$ and $|\Omega|=1/2$, such that, especially for higher rotational levels, Ω is not a good quantum number anymore. However, in the low-J limit, Ω is an approximately good quantum number, and a wave function is labeled with F_1 when it corresponds to $|\Omega|=3/2$ and with F_2 when it corresponds with $|\Omega|=1/2$.

C. Line intensities and Einstein A coefficients

The line intensity $S_{\mathbf{ul}}(T)$ in $\mathrm{cm}^2/(\mathrm{s\ molecule})$ for a photoabsorption transition $|\mathbf{u}\rangle \leftarrow |\mathbf{l}\rangle$ from a lower state $|\mathbf{l}\rangle$ to an upper state $|\mathbf{u}\rangle$ is given by[21]

$$S_{\mathbf{ul}}(T) = \frac{e^{-E_\mathbf{l}/k_\mathrm{b}T} - e^{-E_\mathbf{u}/k_\mathrm{b}T}}{Q(T)} I_a g_\mathbf{l} \bar{\sigma}_{\mathbf{ul}}(\omega_0). \tag{13}$$

Here, the exponentials are Boltzmann factors for lower and upper states at temperature T, $Q(T)$ is the molecular partition function, $g_\mathbf{l}$ is the degeneracy of the lower state, and $I_a=0.997\,473$ is the ^{16}OH isotope abundance. The transitions are labeled with $\mathbf{u}$ and $\mathbf{l}$, which denote the set of quantum numbers in upper and lower states that are resolved in experiment or calculation. Here, we have $\mathbf{u}=\{v,J,F_n,p\}$ and $\mathbf{l}=\{v',J',F_{n'},p'\}$. The integrated line photoabsorption cross section $\bar{\sigma}(\omega_0)$ $(\mathrm{cm}^2/\mathrm{s})$ at the angular transition frequency ω_0 (s^{-1}) is given by

$$\bar{\sigma}_{\mathbf{ul}}(\omega_0) = \frac{4\pi^2\alpha\omega_0}{(2J'+1)e^2} \sum_{M_J M_{J'}} |\langle \psi^{JM_J}_{vF_np}|\hat{\boldsymbol{\varepsilon}}\cdot\boldsymbol{\mu}|\psi^{J'M_{J'}}_{v'F_{n'}p'}\rangle|^2, \tag{14}$$

where we average over lower, and sum over upper degenerate states. Furthermore, α is the fine-structure constant, e the

TABLE II. Experimental and computed vibrational energy levels G_v in cm^{-1}. Computed results are shown for the scaled potential $V_{sc}(r)$ [see Eq. (11)] and for the original *ab initio* potential $V(r)$. The coefficients are given in Table III.

	Expt.	*Ab initio*		Scaled	
	G_v[a]	G_v	Error (%)	G_v	Error (%)
v					
0	0	0	0	0	0
1	3 569.6415	3 573.2426	0.101	3 569.4944	-4.121×10^{-3}
2	6 973.6790	6 981.1031	0.107	6 973.6800	1.501×10^{-5}
3	10 214.0371	10 225.0300	0.108	10 214.0972	5.884×10^{-4}
4	13 291.8106	13 305.9995	0.107	13 291.8158	3.873×10^{-5}
5	16 207.1007	16 224.1848	0.105	16 207.1571	3.477×10^{-4}
6	18 958.7928	18 978.0894	0.102	18 958.7717	-1.114×10^{-4}
7	21 544.2632	21 565.0051	0.096	21 544.1885	-3.468×10^{-4}
8	23 958.9883	23 980.2775	0.089	23 959.0303	1.754×10^{-3}
9	26 196.0203	26 216.2050	0.077	26 196.0135	-2.607×10^{-5}
10	28 245.2835	28 262.3640	0.060	28 245.2872	1.308×10^{-5}

[a]Reference 58.

elementary charge, $\hat{\boldsymbol{\varepsilon}}$ is the photon polarization vector, and μ is the electric dipole operator given by $\mu_q^{(1)}=\Sigma_t d_t^{(1)} D_{qt}^{(1)*}(\alpha,\beta,0)$, where $\mathbf{d}$ is the electric dipole operator in the molecular frame. Choosing the laboratory Z axis along the photon polarization, integrating over angles α and β, and completing the sum over M_J and $M_{J'}$ gives

$$\bar{\sigma}_{\mathbf{ul}}(\omega_0)=\frac{4\pi^2\alpha\omega_0}{3(2J'+1)e^2}|\langle\psi^J_{vF_np}\|d^{(1)}\|\psi^{J'}_{v'F_{n'}p'}\rangle|^2, \tag{15}$$

where the reduced matrix element reads

$$\langle\psi^J_{vF_np}\|d^{(1)}\|\psi^{J'}_{v'F_{n'}p'}\rangle = (2J+1)^{1/2}\sum_{\Omega=1/2,3/2}\langle J\Omega 10|J'\Omega\rangle\langle f^{J|\Omega|}_{vF_np}|d_0^{(1)}|f^{J'|\Omega|}_{v'F_{n'}p'}\rangle_r. \tag{16}$$

The Einstein A coefficient in s^{-1} for the spontaneous emission process $|\mathbf{u}\rangle\rightarrow|\mathbf{l}\rangle$ is connected to the line intensity by

$$S_{\mathbf{ul}}(T)=\frac{e^{-E_\mathbf{l}/k_bT}-e^{-E_\mathbf{u}/k_bT}}{Q(T)}\frac{I_a\pi^2c^2g_\mathbf{u}}{\omega_0^2}A_{\mathbf{ul}}, \tag{17}$$

where c is the speed of light, and it follows that $A_{\mathbf{ul}}$ is given by

$$A_{\mathbf{ul}}=\frac{2J'+1}{2J+1}\frac{\omega_0^2}{c^2\pi^2}\bar{\sigma}_{\mathbf{ul}}(\omega_0). \tag{18}$$

The radiative lifetime $\tau_\mathbf{u}$ (in seconds) of an upper state $|\mathbf{u}\rangle$ reads

$$\tau_\mathbf{u}^{-1}=\sum_\mathbf{l}A_{\mathbf{ul}}, \tag{19}$$

where the sum is over al states $|\mathbf{l}\rangle$ with $E_\mathbf{l}<E_\mathbf{u}$. Finally, we note that line strengths S are often given in $cm^2/(cm\ molecule)$, instead of $cm^2/(s\ molecule)$. In that case ω_0 in Eqs. (13)–(18) must be replaced by the wave number ν_0 given by $\nu_0=\omega_0/(100\times2\pi c)$.

III. RESULTS

A. Potential energy curve

In Table II, the computed and experimental vibrational band origins G_v are shown. The coefficients we found for the scaling procedure [see Eq. (11)] are shown in Table III. Even though the scaling has a small effect on the shape of the potential [the case of no scaling is equivalent to coefficients $(c_0,c_1,c_2,c_3)=(0,1,0,1)$], the reduction in error is large. The relative errors are reduced by at least two orders of magnitude with respect to the fully *ab initio* potential, yielding relative errors on the order of 10^{-5} or less. The difference between experimental and computed vibrational levels is 0.14 cm^{-1} for $v=1$ and less than 0.07 cm^{-1} for $v=2-10$. This is about an order of magnitude more accurate than the vibrational levels computed by Langhoff *et al.*[38] who used the RKR potential of Coxon and Foster,[56] extended with a scaled *ab initio* potential to describe the potential at large interatomic separations. In total, we found 17 bound vibrational levels, while Langhoff *et al.* found 16. Our *ab initio* potential energy curve has an r_e value of $1.8334a_0$, which differs only by $8\times10^{-4}a_0$ from the experimental value[51] of $1.8342a_0$. After fitting c_1, c_2, and c_3, but keeping $c_0=0$, the potential has a slightly shifted r_e value of $1.8314a_0$, yielding a c_0 value of $2.8\times10^{-3}a_0$.

B. Dipole moment function

In Fig. 1, five dipole moment functions from the literature are compared with ours. The dipole moment functions are in general very similar except in the outer regions where

TABLE III. Coefficients for the scaled potential $V_{sc}(r)$ in Eq. (11).

	Scaling constants
c_0	2.8×10^{-3}
c_1	1.005 123 15
c_2	$-2.202\ 238\ 46\times10^{-3}$
c_3	1.003 899 25

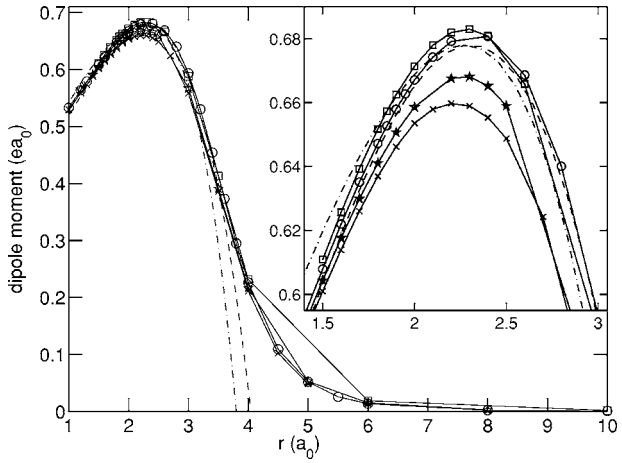

FIG. 1. Dipole moment functions of OH compared. *Ab initio* points are connected here by straight lines, in our calculations we use an interpolation scheme. This work (⊙), Langhoff *et al.* (Ref. 39) (1989) (□), Langhoff *et al.* (Ref. 38) (1986) (×), Werner *et al.* (Ref. 37) (⋆), experimental curve by Nelson *et al.* (Ref. 31) (--), and experimental curve by Murphy (Ref. 20) (-·). The curve of Murphy is determined up to a constant and was shifted up by about $0.85ea_0$ for graphical reasons.

the fitted curves of Murphy[20] and Nelson *et al.*[31] decrease too fast as a function of r. This is a consequence of the functional form used to determine these functions: a fifth order polynomial for Murphy's and a third order polynomial for the electric dipole moment function of Nelson *et al.* Nelson *et al.* stated that their electric dipole moment function is valid between $1.32a_0$ and $3.33a_0$, the classical turning points of the $v=9$ level. The dipole moment computed in this work follows the empirical function of Nelson *et al.* most closely in the inner region. This is shown more clearly in Fig. 2, where we plot the difference between Nelson's dipole moment function and a number of *ab initio* computed functions. It can be seen that in the inner region, both the dipole moments by Langhoff *et al.* and by Werner *et al.* cross the empirical function, whereas ours remains slightly above the empirical one. Using a cubic spline interpolation procedure, we find that the maximum of our dipole moment lies at exactly the same interatomic distance as that of Nelson *et al.*, $2.300a_0$, whereas the electric dipole moment function of Longhoff *et al.* has a maximum at $2.2850a_0$ and that of Werner *et al.* at $2.2670a_0$. A scaled and shifted form of the dipole moment function of Werner *et al.* was used in the last extensive fully *ab initio* calculation on the OH Meinel system in 1986.[38]

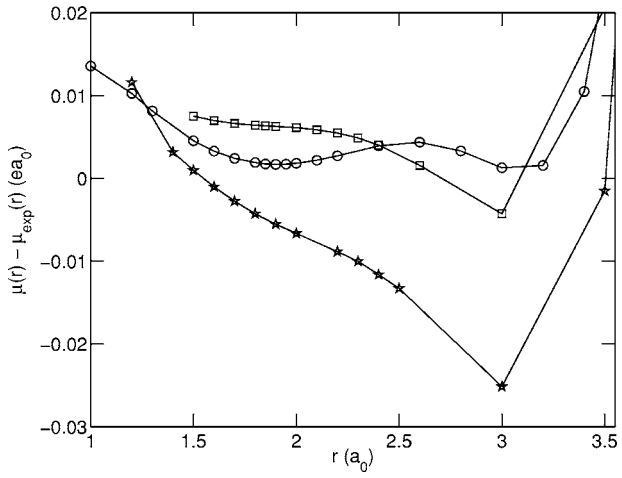

FIG. 2. Difference between *ab initio* electric dipole moment functions and the "experimental" dipole moment function of Nelson *et al.* (Ref. 31). This work (⊙), Langhoff *et al.* (Ref. 39) (1989) (□), and Werner *et al.* (Ref. 37) (⋆).

TABLE IV. Computed and experimental vibrationally averaged dipole moments of OH in ea_0.

v	Expt.[a]	Present	L89[b]	WRR[c]
0	0.651 20(4)	0.6530	0.6573	0.6460
1	0.654 11(6)	0.6564	0.6601	0.6483
2	0.655 0(4)	0.6584	0.6613	0.6491
3		0.6587	0.6607	0.6481
4		0.6568	0.6579	0.6449
5		0.6522	0.6525	0.6390
6		0.6443	0.6438	0.6296
7		0.6322	0.6311	0.6159
8		0.6150	0.6134	0.5972
9		0.5914	0.5898	0.5726

[a]Peterson *et al.* (Ref. 57). Converted from Debye using 1 D $=0.393\,430\,313\,69ea_0$.
[b]Langhoff *et al.* (Ref. 39).
[c]Werner *et al.* (Ref. 37).

One of the most stringent tests on the quality of the *ab initio* calculated dipole moment function is comparing vibrationally averaged dipole moments with the very accurate measurements of Peterson *et al.*[57] The experimentally determined dipole moments are accurate up to $10^{-5}ea_0$ for $v=0$ and $v=1$ and $10^{-4}ea_0$ for $v=2$. In all references cited here, the comparison of experimental with *ab initio* computed dipole moments was done after shifting and/or scaling the *ab initio* dipole moment functions. Here, we compute the vibrationally averaged dipole moments without any scaling of the dipole moment function. For comparison, we also computed this property using some previously published dipole moment functions. The results are shown in Table IV. It can be seen that our dipole moment function yields values in very close agreement with the experimental results, with differences between experiment and *ab initio* results of about $0.0020ea_0$ for the $v=0$ and $v=1$ levels and $0.034ea_0$ for $v=3$.

C. Lifetimes

In the first and second column of Table V we show the lifetime of the OH$(v=1,J=3/2,F_1,p)$ states, which are the only states of which the lifetimes have been determined directly by experiment.[11] The lifetimes have been computed using different dipole moment functions and methods and are compared with the two best-known current values: the direct measurement of van de Meerakker *et al.*[11] and the value which can be extracted from the high-resolution transmission molecular absorption (HITRAN) 2004 database using Eqs. (17) and (19). The HITRAN values we use here are ultimately based on the calculation by Goldman *et al.*[29]

The dipole moment functions by Langhoff *et al.* (L86), Murphy (M71), and Werner *et al.* (WRR) give lifetimes

TABLE V. Lifetime of the OH($v=1, J=3/2, F_1, p$) states, computed using various dipole moment functions and methods.

Expt.	$e(-)$	$f(+)$	Error bars	
Direct[a]	59.0		±2 ms	
HITRAN[b]	58.1528	58.1457	±10%–20%	
Calc.	$H_{so}(r)$		$H^{so}_{\|\Omega\|,\|\Omega'\|}$	
	$e(-)$	$f(+)$	$e(-)$	$f(+)$
Present[c]	58.2517	58.2501	58.1949	58.1934
Nosc[d]	58.4786	58.4770	58.4217	58.4202
ω_H[e]	58.2350	58.2347	58.1831	58.1828
N90[f]	57.0505	57.0490	56.9941	56.9926
L89[g]	59.1897	59.1881	59.1308	59.1292
WRR[h]	73.4544	73.4523	73.3803	73.3783
L86[i]	83.3714	83.3689	83.2845	83.2821
M71[j]	87.9550	87.9523	87.8655	87.8629

[a]Experiment by van de Meerakker *et al.* (Ref. 11).
[b]Computed from the HITRAN 2004 (Ref. 59) database.
[c]This work, using the scaled potential.
[d]This work, using the *initio* potential.
[e]This work, using HITRAN transition frequencies.
[f]Fitted dipole moment function by Nelson *et al.* (Ref. 31).
[g]*Ab initio* dipole moment function by Langhoff *et al.* (Ref. 39) (1989).
[h]*Ab initio* dipole moment function by Werner *et al.* (Ref. 37).
[i]*Ab initio* dipole moment function by Langhoff *et al.* (Ref. 38) (1986).
[j]Fitted dipole moment function by Murphy (Ref. 20) (1971).

which differ from the experimental values by about 15–30 ms. The dipole moments of Langhoff *et al.* (L89), Nelson *et al.* (N90), and from this work all give values which are within the experimental errors. Values computed using our dipole moment functions lie between the best known current experimental values, whereas the values obtained from the L89 and N90 dipole moment functions are slightly above or below these values, respectively.

To investigate the effect of scaling the potential, we also compute the lifetimes using wave functions from our potential without scaling it (labeled nosc). We also compute the lifetimes using our wave functions and the transition frequencies taken from HITRAN (labeled ω_H) to distinguish overlap effects from energy level effects. The difference in lifetime for these two methods is about 0.025 ms. This indicates that rovibrational wave functions are well represented in our calculation. Thus, we expect the error in lifetimes caused by the error in calculated transition frequencies to be on the order of 0.05%.

In Fig. 3, we show the r-dependent spin-orbit coupling $H_{so}(r)$. The spin-orbit coupling matrix element rises steeply between $2.8a_0$ and about $5.5a_0$. At $7.0a_0$ the spin-orbit coupling is within 1 cm^{-1} of its asymptotic value, -100.74 cm^{-1} at $16a_0$. The vibrationally averaged spin-orbit splitting is -135.48 cm^{-1} for $v=0$, which is close to the experimental spectroscopic A constant shown in Table I. From $v=1$ to $v=8$ the vibrationally averaged spin-orbit splitting increases from -135.79 to -137.09 cm^{-1}. For $v=9-10$ the splitting decreases again to -136.63 cm^{-1} for $v=10$. This behavior is consistent with the spin-orbit A constants, shown in Table I.

In the third and fourth column of Table V we compare the lifetimes computed using the r-independent spin-orbit Hamiltonian [$H^{so}_{|\Omega|,|\Omega'|}$, Eq. (7)] with the values obtained using $H_{so}(r)$. Since the transition frequencies are slightly different when $H^{so}_{|\Omega|,|\Omega'|}$ is used instead of $H_{so}(r)$, we also compare with the ω_H calculation. We conclude that replacing the r-dependent spin-orbit coupling with the parametrized Hamiltonian decreases the computed lifetime of OH[$X\,^2\Pi(v=1, J=3/2)$] by about 0.05 ms. Calculations for higher rovibrational levels show that this effect decreases exponentially as the rotational or vibrational level increases. In the $v=1$, $J=41/2$ state, the difference in lifetime, computed with $H_{so}(r)$ versus $H^{so}_{|\Omega|,|\Omega'|}$ is 9×10^{-4} ms, about 0.013% of the lifetime of that state. In the $v=9$, $J=3/2$ state this difference is about 0.0019 ms, about 0.036% of the lifetime of that state. The effect that the approximate $H^{so}_{|\Omega|,|\Omega'|}$ Hamiltonian yields better results for higher excited states can be explained by the notion that higher excited rovibrational states probe larger internuclear distances, where the spin-orbit coupling becomes constant. Also, higher excited vibrational levels have more kinetic energy, so the approximation of a vibrationally averaged spin-orbit coupling becomes better at higher excited rovibrational states.

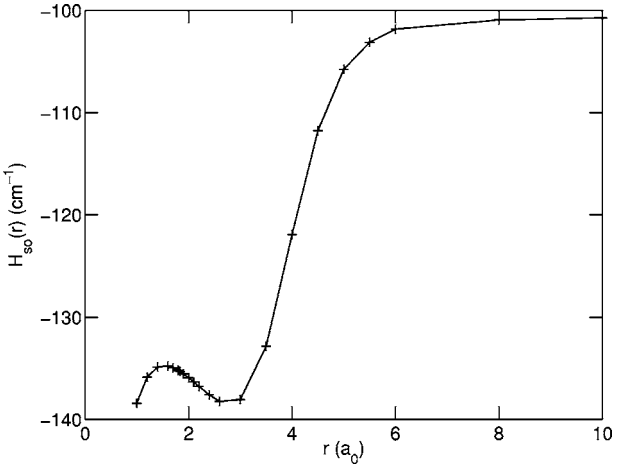

FIG. 3. r-dependent spin-orbit coupling computed in this work.

Using our electric dipole moment and scaled potential energy curve, we computed a total of 24 660 photoabsorption cross sections and Einstein A coefficients, which can be retrieved via the EPAPS (Ref. 52) system in ASCII format. The file contains the cross sections $\bar{\sigma}_{\mathbf{ul}}$ as defined in Eq. (14), the Einstein A coefficients defined in Eq. (19), the full set of quantum numbers $\{v, J, F_n, p\}$ for upper and lower states, the transition energy, and the energy of the lower state with respect to the dissociation energy D_e. We include vibrational levels $v=0-10$ and rotational levels up to and including $J=121/2$. The potential energy curve, electric dipole moment function, and spin-orbit coupling function are also included in the EPAPS data.

IV. CONCLUSION

We computed a new, accurate *ab initio* potential energy curve, electric dipole moment function, and spin-orbit coupling function for OH($X\,^2\Pi$). Both the calculated permanent vibrationally averaged dipole moments and spin-orbit couplings are computed with unprecedented precision. The ef-

fect of the OH bond length dependence of the spin-orbit coupling is investigated, and we conclude that the maximum variation in lifetimes is on the order of 0.1 ms (about 0.1%). The effect decreases exponentially as the rotational or vibrational quantum number increases. The effect of lambda-type doubling on the mixing of states with different Ω quantum numbers is incorporated for the first time. We report a new set of accurate photoabsorption cross sections and Einstein *A* coefficients, available via the EPAPS (Ref. 52) system.

ACKNOWLEDGMENTS

The authors are greatly indebted to Professor Philip Cosby for providing us with the details of the spectroscopic Hamiltonian and the preprint of his paper. The authors thank Professor Ad van der Avoird for carefully reading the manuscript. This research has been financially supported by the Council for Chemical Sciences of the Netherlands Organization for Scientific Research (CW-NWO).

[1] A. B. Meinel, Astrophys. J. **111**, 555 (1950).
[2] F. Phillips, G. B. Burns, W. J. R. French, P. F. B. Williams, A. R. Klekociuk, and R. P. Lowe, Ann. Geophys. **22**, 1549 (2004).
[3] H. M. Pickett, W. G. Read, K. K. Lee, and Y. L. Yung, Geophys. Res. Lett. **33**, 19808 (2006).
[4] R. A. Viereck and C. S. Deehr, J. Geophys. Res. **94**, 5397 (1989).
[5] U. B. Makhlouf, R. H. Picard, and J. R. Winick, J. Geophys. Res. **100**, 11289 (1995).
[6] G. R. Swenson and C. S. Gardner, J. Geophys. Res. **103**, 6271 (1998).
[7] D. L. Huestis, S. K. Atreya, S. J. Bolton *et al.*, Bull. Am. Astron. Soc. **33**, 1055 (2001).
[8] A. García Muñoz, J. C. McConnell, I. C. McDade, and S. M. L. Melo, Icarus **176**, 75 (2005).
[9] J. Meléndez, B. Barbuy, and F. Spite, Astrophys. J. **556**, 858 (2001); e-print astro-ph/0104184.
[10] S. Y. T. van de Meerakker, P. Smeets, N. Vanhaecke, R. T. Jongema, and G. Meijer, Phys. Rev. Lett. **94**, 023004 (2005).
[11] S. Y. T. van de Meerakker, N. Vanhaecke, M. P. J. van der Loo, G. C. Groenenboom, and G. Meijer, Phys. Rev. Lett. **95**, 013003 (2005).
[12] V. I. Shklovskii, Dokl. Akad. Nauk SSSR **80**, 735 (1950).
[13] J. W. Chaimberlain and C. A. Smith, J. Geophys. Res. **64**, 611 (1959).
[14] G. Kvifte, Planet. Space Sci. **5**, 158 (1961).
[15] H. S. Heaps and G. Herzberg, Z. Phys. **133**, 48 (1952).
[16] J. Wallace, J. Atmos. Sci. **19**, 1 (1962).
[17] D. Garvin, H. P. Broida, and H. J. Kostowski, J. Chem. Phys. **32**, 880 (1960).
[18] A. F. Ferguson and D. Parkinson, Planet. Space Sci. **11**, 149 (1963).
[19] V. I. Krassovsky, Dokl. Akad. Nauk SSSR **80**, 735 (1951).
[20] R. E. Murphy, J. Chem. Phys. **54**, 4852 (1971).
[21] L. Rothman, C. P. Rinsland, A. Goldman *et al.*, J. Quant. Spectrosc. Radiat. Transf. **60**, 665 (1998).
[22] J. Gilles and A. Goldman, J. Quant. Spectrosc. Radiat. Transf. **26**, 23 (1980).
[23] A. Goldman, Appl. Opt. **21**, 2100 (1982).
[24] A. Goldman, J. R. Gilles, and J. A. Coxon, J. Quant. Spectrosc. Radiat. Transf. **29**, 469 (1983).
[25] F. Mies, J. Mol. Spectrosc. **53**, 150 (1974).
[26] D. Turnbull and R. Lowe, Planet. Space Sci. **37**, 723 (1989).
[27] P. C. Cosby and T. G. Slanger, Can. J. Phys. (to be published).
[28] V. I. Krassovsky, N. Shefov, and V. Yarin, Planet. Space Sci. **9**, 883 (1962).
[29] A. Goldman, W. G. Schoenfeld, D. Goortvitch, C. Chackerian, Jr., H. Dothe, F. Mélen, M. C. Abrams, and J. E. A. Selby, J. Quant. Spectrosc. Radiat. Transf. **59**, 453 (1998).
[30] D. D. Nelson, Jr. and A. D. J. Nesbitt, J. Chem. Phys. **90**, 5443 (1989).
[31] D. D. Nelson, Jr., A. Schiffman, D. J. Nesbitt, J. J. Orlando, and J. B. Burkholder, J. Chem. Phys. **93**, 7003 (1990).
[32] J. A. Coxon and S. C. Foster, J. Mol. Spectrosc. **91**, 243 (1982).
[33] P. C. Cosby, T. G. Slanger, and D. L. Huestis, The 55th Ohio State University International Symposium on Molecular Spectroscopy, 2000 (unpublished), http://spectroscopy.mps.ohio-state.edu/symposium_55/symposium/Program/TA.html#TA01
[34] R. Colin, P.-F. Coheur, M. Kiseleva, A. C. Vandaele, and P. F. Bernath, J. Mol. Spectrosc. **214**, 225 (2002).
[35] M. C. Abrams, S. P. Davis, M. Rao, R. Engleman, Jr., and J. W. Brault, Astrophys. J., Suppl. Ser. **93**, 351 (1994).
[36] W. J. Stevens, G. Das, A. C. Wahl, M. Krauss, and D. Neumann, J. Chem. Phys. **61**, 3686 (1974).
[37] H.-J. Werner, P. Rosmus, and E.-A. Reinsch, J. Chem. Phys. **79**, 905 (1983).
[38] S. R. Langhoff, H.-J. Werner, and P. Rosmus, J. Mol. Spectrosc. **118**, 507 (1986).
[39] S. R. Langhoff, C. W. Bauschlicher, and P. R. Taylor, J. Chem. Phys. **91**, 5953 (1989).
[40] S. R. Langhoff, C. W. Bauschlicher, and P. R. Taylor, J. Chem. Phys. **86**, 6992 (1987).
[41] E. Hill and J. H. van Vleck, Phys. Rev. **32**, 250 (1928).
[42] M. C. Abrams, S. P. Davis, M. L. P. Rao, and R. Engleman, Jr., J. Mol. Spectrosc. **165**, 57 (1994).
[43] R. N. Zare, A. L. Schmeltekopf, W. J. Harrop, and D. L. Albritton, J. Mol. Spectrosc. **46**, 37 (1973).
[44] H.-J. Werner, P. J. Knowles, R. Lindh *et al.*, MOLPRO, *version 2006, a package of ab initio programs* (2006).
[45] M. P. J. van der Loo and G. C. Groenenboom, J. Chem. Phys. **123**, 074310 (2005).
[46] P. J. Knowles and H.-J. Werner, Chem. Phys. Lett. **145**, 514 (1988).
[47] H.-J. Werner and P. J. Knowles, J. Chem. Phys. **89**, 5803 (1988).
[48] H.-J. Werner and P. J. Knowles, J. Chem. Phys. **82**, 5053 (1985).
[49] P. J. Knowles and H.-J. Werner, Chem. Phys. Lett. **115**, 259 (1985).
[50] T. H. Dunning, J. Chem. Phys. **90**, 1007 (1989).
[51] K. P. Huber and G. Herzberg, *Molecular Spectra and Molecular Structure. IV. Constants of Diatomic Molecules* (Van Nostrand Reinhold, New York, 1979).
[52] See EPAPS Document No. E-JCPSA6-126-017709 for the computed potential energy curve and properties. This document can be reached via a direct link in the online article's HTML reference section section or via the EPAPS homepage (http://www.aip.org/pubservs/epaps.html).
[53] T.-S. Ho and H. Rabitz, J. Chem. Phys. **104**, 2584 (1996).
[54] D. T. Colbert and W. H. Miller, J. Chem. Phys. **96**, 1982 (1992).
[55] G. C. Groenenboom and D. T. Colbert, J. Chem. Phys. **99**, 9681 (1993).
[56] J. A. Coxon and S. C. Foster, Can. J. Phys. **60**, 41 (1982).
[57] K. I. Peterson, G. T. Fraser, and W. Klemperer, Can. J. Phys. **62**, 1502 (1984).
[58] P. C. Cosby (private communication); see also Ref. 33.
[59] L. Rothman, D. Jacquemart, A. Barbe *et al.*, J. Quant. Spectrosc. Radiat. Transf. **96**, 139 (2005).